The Astrophysical Journal, 619:L31–L34, 2005 January 20

THE ULTRAVIOLET LUMINOSITY FUNCTION OF *GALEX* GALAXIES AT PHOTOMETRIC REDSHIFTS BETWEEN 0.07 AND 0.25

Tamás Budavári,[1] Alex S. Szalay,[1] Stéphane Charlot,[2,3] Mark Seibert,[4] Ted K. Wyder,[4] Stéphane Arnouts,[5] Tom A. Barlow,[4] Luciana Bianchi,[1] Yong-Ik Byun,[6] José Donas,[5] Karl Forster,[4] Peter G. Friedman,[4] Timothy M. Heckman,[1] Patrick N. Jelinsky,[7] Young-Wook Lee,[6] Barry F. Madore,[8] Roger F. Malina,[5] D. Christopher Martin,[4] Bruno Milliard,[5] Patrick Morrissey,[4] Susan G. Neff,[9] R. Michael Rich,[10] David Schiminovich,[11] Oswald H. W. Siegmund,[7] Todd Small,[4] Marie A. Treyer,[4,5] and Barry Welsh[7]

Received 2004 May 6; accepted 2004 June 15; published 2005 January 17

ABSTRACT

We present measurements of the UV galaxy luminosity function and the evolution of luminosity density from *Galaxy Evolution Explorer* (*GALEX*) observations matched to the Sloan Digital Sky Survey (SDSS). We analyze galaxies in the Medium Imaging Survey overlapping the SDSS First Data Release, with a total coverage of 44 deg^2. Using the combined *GALEX* + SDSS photometry, we compute photometric redshifts and study the luminosity function in three redshift shells between $z = 0.07$ and 0.25. The Schechter function fits indicate that the faint-end slope α is consistent with -1.1 at all redshifts, but the characteristic UV luminosity M_* brightens by 0.2 mag from $z = 0.07$ to 0.25. In the lowest redshift bin, early- and late-type galaxies are studied separately, and we confirm that red galaxies tend to be brighter and have a shallower slope α than blue ones. The derived luminosity densities are consistent with other *GALEX* results based on a local spectroscopic sample from the Two-Degree Field, and the evolution follows the trend reported by deeper studies.

Subject headings: galaxies: evolution — galaxies: luminosity function, mass function — galaxies: photometry — surveys — ultraviolet: galaxies

1. INTRODUCTION

In the era of precision cosmology, the star formation history of the universe can be studied accurately as one is able to detect evolutionary effects in the observables on top of the global expansion. In particular, the rest-frame ultraviolet luminosity of galaxies has proven to yield a good handle on the star formation rate (Kennicutt 1998). A number of galaxy surveys have probed the history of star formation at different redshifts. While most studies agree on a relatively rapid rise in the star formation rate (SFR) out to a redshift of $z \sim 1$, significant uncertainties remain even at lower redshifts (Lilly et al. 1996; Connolly et al. 1997; Cowie et al. 1999; Wilson et al. 2002). The rest-frame UV continuum of local galaxies is not accessible from the ground. The balloon-borne telescope of the FOCA experiment (Milliard et al. 1992) had been the best window onto the UV sky until last year, when the *Galaxy Evolution Explorer* (*GALEX*) satellite was successfully launched to orbit. This Letter is one of the first in a series of luminosity function papers on *GALEX* sources, and it focuses on galaxies at redshifts between $z = 0.07$ and 0.25. We use photometric redshifts to boost our sample size by a factor of 20, compared to spectroscopic data available. Throughout the Letter, we assume a flat ΛCDM cosmology with $\Omega_M = 0.3$ and $H_0 = 70$ km s^{-1} Mpc^{-1}.

[1] Department of Physics and Astronomy, Johns Hopkins University, 3701 San Martin Drive, Baltimore, MD 21218.
[2] Max-Planck-Institute für Astrophysik, D-85748 Garching, Germany.
[3] Institut d'Astrophysique de Paris, CNRS, 98 Bis Boulevard Arago, F-75014 Paris, France.
[4] California Institute of Technology, MC 405-47, 1200 East California Boulevard, Pasadena, CA 91125.
[5] Laboratoire d'Astrophysique de Marseille, BP 8, Traverse du Siphon, 13376 Marseille Cedex 12, France.
[6] Center for Space Astrophysics, Yonsei University, Seoul 120-749, Korea.
[7] Space Sciences Laboratory, University of California at Berkeley, 601 Campbell Hall, Berkeley, CA 94720.
[8] Observatories of the Carnegie Institution of Washington, 813 Santa Barbara Street, Pasadena, CA 91101.
[9] Laboratory for Astronomy and Solar Physics, NASA Goddard Space Flight Center, Greenbelt, MD 20771.
[10] Department of Physics and Astronomy, University of California, Los Angeles, CA 90095.
[11] Department of Astronomy, Columbia University, New York, NY 10027.

2. THE SAMPLE

The *GALEX* telescope has two photometric bands at 1530 Å (far-UV; FUV) and 2310 Å (near-UV; NUV) and a 1.°2 field of view. For a detailed description of survey and performance, see Martin et al. (2005) and Morrissey et al. (2005) in the present volume. Our sample consists of Medium Imaging Survey (MIS) fields overlapping with the First Data Release (DR1) coverage of the Sloan Digital Sky Survey (SDSS; Abazajian et al. 2003; see also Seibert et al. 2005). The depth of the MIS fields is well matched to SDSS, and this unique seven-band multicolor data set provides a good basis for various statistical studies. We select the 57 fields with more than 1400 s exposure times and no objects with higher extinction than $E(B - V) = 0.08$. We use 36′ radius circles in the center of the fields to ensure uniform image quality. The intersection of the unique area of these MIS fields with the SDSS DR1 footprint is 43.9 deg^2. Our catalog contains only objects that are classified as galaxies by the SDSS photometric pipeline based on their morphology. We use total magnitudes corrected for foreground extinction: SExtractor's MAG_AUTO for *GALEX* and model magnitudes from SDSS. For the limiting magnitudes, we choose a safe $m_{\rm lim} = 21.5$ cut in both bands to ensure completeness (Xu et al. 2005).

2.1. *Photometric Redshifts*

Photometric redshifts are utilized to fully exploit the data set. We choose empirical photometric redshifts over template-based estimates, because currently the *GALEX* photometric system is only known to about 10% accuracy, and spectral energy distribution (SED) fitting is sensitive to zero-point errors. Following Connolly et al. (1995), a third-order polynomial formula was

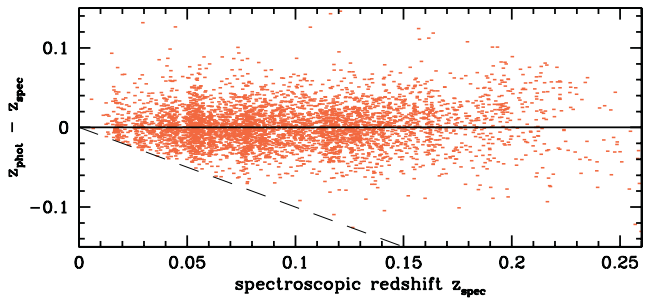

FIG. 1.—Comparison of the spectroscopic and photometric redshifts for the MIS objects in our training set. Black dashed line shows $z_{phot} = 0$.

applied to map the *GALEX* NUV and SDSS $u'g'r'i'z'$ magnitudes to photometric redshifts. Note that the FUV magnitude was excluded from the fitting formula as the NUV observations go deeper, and not all galaxies have FUV measurements. This way there is only one redshift estimator that can be used for both FUV- and NUV-limited samples. We find that the empirical fit yields reliable redshift estimates out to a redshift of 0.25. For the training set of 6295 galaxies, the rms scatter is $\Delta z_{rms} = 0.026$, and about 2% are outliers. This accuracy is about 15% better than SDSS alone, using the same technique. A more detailed analysis and a photometric redshift catalog will be published elsewhere (T. Budavári et al. 2004, in preparation). We expect the uncertainty in the photometric redshifts to be a significant source of error in our statistical analysis, so we adopt a conservative nominal redshift error of $\sigma_z = 0.03$. Figure 1 compares the spectroscopic and photometric redshifts as a function of redshift.

One of the disadvantages of the empirical photometric redshifts is that the method does not provide a direct measurement of the spectral types or *K*-corrections. To overcome this, we fitted synthetic-model spectra with full wavelength coverage from the UV to IR to the SDSS photometry, and picked the best-fitting template for each galaxy. Our template set has 10 interpolated spectra from Ell to Irr of Bruzual & Charlot (2003). For each of these templates, the *K*-correction is calculated as a function of redshift. In addition to the galaxy templates, we also include a series of QSO spectra in an attempt to identify active galactic nuclei (AGNs) in the sample. Those objects that are best-fitted with quasar templates (roughly 10%) are removed from the sample. Our photometric redshift catalog contains 190,489 MIS galaxies, out of which 9356 pass the area, magnitude, redshift, and SED cuts in the NUV, and 6174 in the FUV.

3. LUMINOSITY FUNCTION RESULTS

There are several methods for calculating the luminosity function (LF; Schmidt 1968; Lynden-Bell 1971; Choloniewski 1986; Subbarao et al. 1996). We use the V_{max} method (Schmidt 1968) to calculate the LF in 0.1 mag wide bins. First, we derive the absolute magnitude using the distance modulus and the *K*-correction, then the maximum redshift at which the object could be observed. The LF is then calculated as $\phi(M)\,dM = \sum 1/V(z_{max})$, where $V(z) = (\Omega/3)d^3(z)$ for a flat universe, Ω is the areal coverage, and $d(z)$ is the comoving distance.

To estimate the uncertainty in the LF, we create 50 Monte

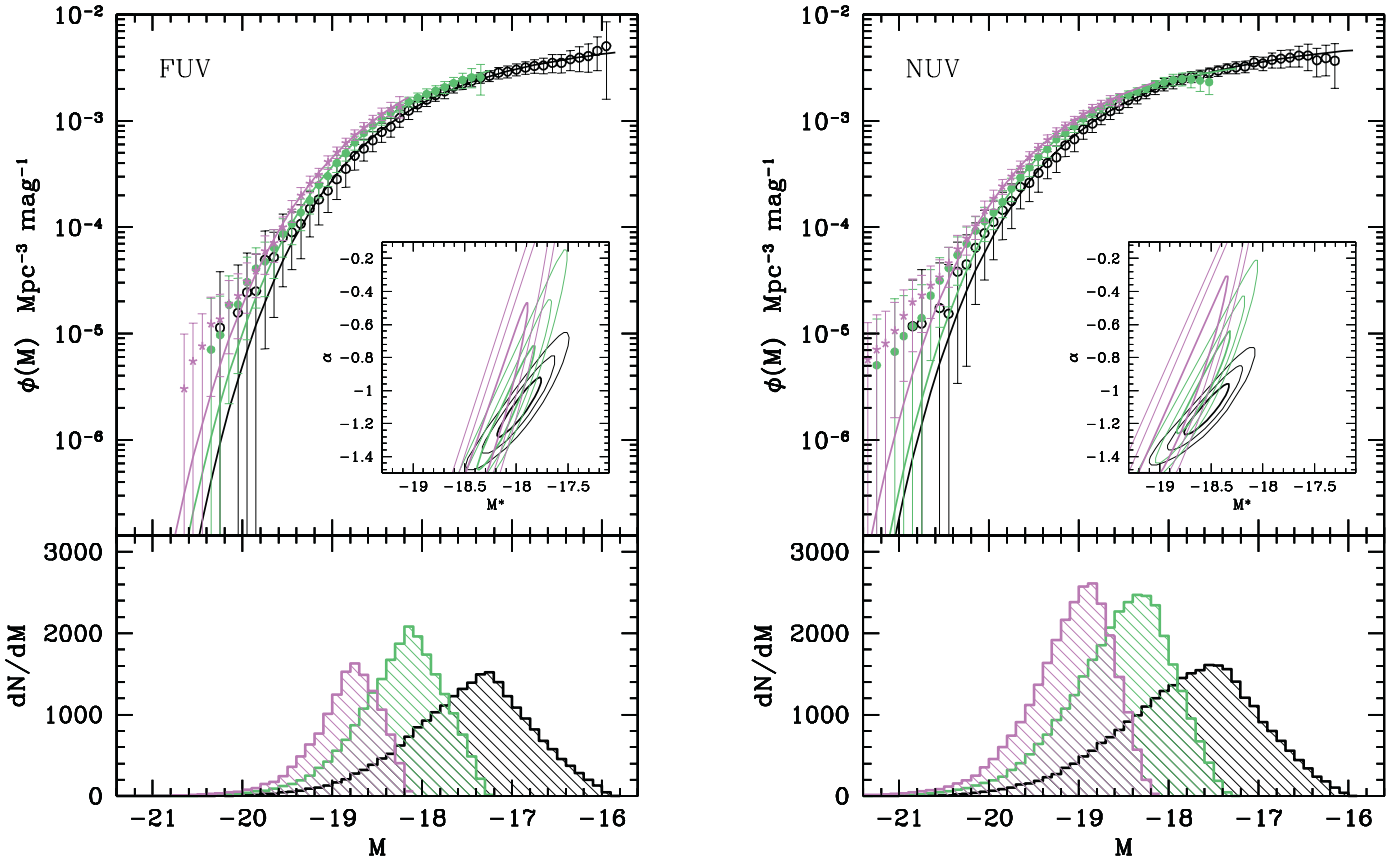

FIG. 2.—*GALEX* FUV and NUV luminosity functions in three redshift bins (*black open circle s*: $0.07 < z < 0.13$; *green solid circles*: $0.13 < z < 0.19$; *magenta stars*: $0.19 < z < 0.25$). The top panel illustrates the $1/V_{max}$ measurements, along with the best-fitting Schechter functions. The confidence regions on M_* and α are shown in the insets. The bottom panel shows the number of objects involved in the analysis for a particular selection.

TABLE 1
SCHECHTER PARAMETERS AND LUMINOSITY DENSITY

Passband	Redshift	Type	M_*	α	lg ϕ_* (Mpc^{-3})	lg ρ_L (ergs s^{-1} Hz^{-1} Mpc^{-3})
FUV	0.07–0.13	All	-17.97 ± 0.14	-1.10 ± 0.12	-2.35 ± 0.07	$25.51 \pm 0.02 \pm 0.06$
	0.13–0.19	...	-18.07 ± 0.17	-1.09 ± 0.23	-2.33 ± 0.07	$25.58 \pm 0.07 \pm 0.04$
	0.19–0.25	...	-18.15 ± 0.17	-1.03 ± 0.34	-2.35 ± 0.06	$25.61 \pm 0.12 \pm 0.03$
	0.07–0.13	Early	-17.98 ± 0.20	-0.80 ± 0.19	-2.74 ± 0.08	$25.06 \pm 0.02 \pm 0.06$
	0.07–0.13	Late	-17.74 ± 0.19	-1.12 ± 0.17	-2.47 ± 0.09	$25.31 \pm 0.04 \pm 0.06$
NUV	0.07–0.13	All	-18.54 ± 0.15	-1.12 ± 0.10	-2.38 ± 0.07	$25.71 \pm 0.02 \pm 0.06$
	0.13–0.19	...	-18.57 ± 0.17	-0.97 ± 0.20	-2.33 ± 0.07	$25.74 \pm 0.05 \pm 0.04$
	0.19–0.25	...	-18.74 ± 0.23	-0.99 ± 0.35	-2.39 ± 0.08	$25.79 \pm 0.10 \pm 0.03$
	0.07–0.13	Early	-18.53 ± 0.23	-0.73 ± 0.21	-2.66 ± 0.08	$25.35 \pm 0.03 \pm 0.06$
	0.07–0.13	Late	-18.11 ± 0.17	-1.09 ± 0.14	-2.48 ± 0.08	$25.43 \pm 0.03 \pm 0.06$

Carlo (MC) realizations of the catalogs, drawing the redshifts randomly from Gaussian distributions with means of the originally estimated redshifts and widths of $\sigma_z = 0.03$. We co-add the MC realizations for a more robust estimate of the true LF. This method allows us to propagate the errors. The error bars plotted in the figures are combinations of the variations among the MC realizations and the Poisson errors added in quadrature.

3.1. *Evolution with Redshift and Spectral Type*

To study the evolution of the UV LF as a function of redshift, we split the sample into three redshift shells. These low-, medium-, and high-redshift subsamples have galaxies in the 0.07–0.13, 0.13–0.19, and 0.19–0.25 intervals. Figure 2 shows the FUV and NUV LFs for the three redshift slices, along with their best-fitting Schechter (1976) functions. The absolute magnitude range over which the luminosity functions can be fitted is limited at the faint end by the lower redshift cutoff in the more distant shells and also at the bright end at $M \lesssim -20$, where the measurements depart from the Schechter function. The latter is due to residual contamination from QSO light that the SED fitting could not eliminate completely. The insets show the 1, 2, and 3 σ confidence regions on the M_*-α plane. As seen in Figure 2, there is a modest evolution in M_* with redshift in both bands, but the leverage is not enough to constrain α to high accuracy at higher redshifts. In all cases, the slope is consistent with $\alpha = -1.1$. Table 1 lists the Schechter parameters.

We further divide the lowest redshift NUV- and FUV-limited samples into two spectral classes, based on the assigned SEDs. The early-type galaxy class consists of objects with the five reddest templates, and late-type galaxies with the five bluer SEDs, which corresponds to a rest-frame color cut of $(u' - r')_0 = 1.7$. This technique is expected to be more robust than the actual

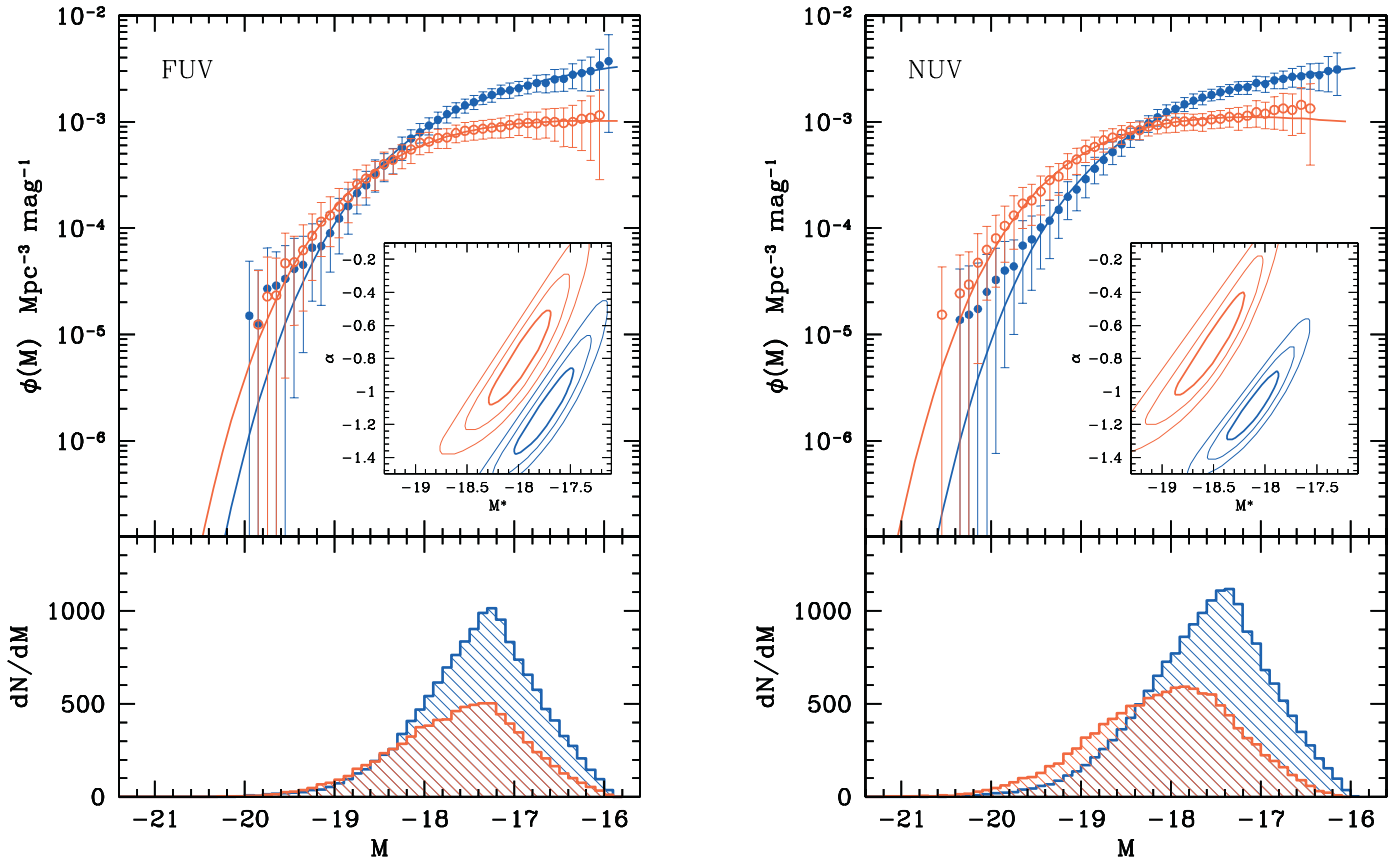

FIG. 3.—Luminosity functions differ in both passbands for the early- and late-type galaxies in the lowest redshift shell. The red galaxy population is brighter and has a shallower faint-end slope than the blue.

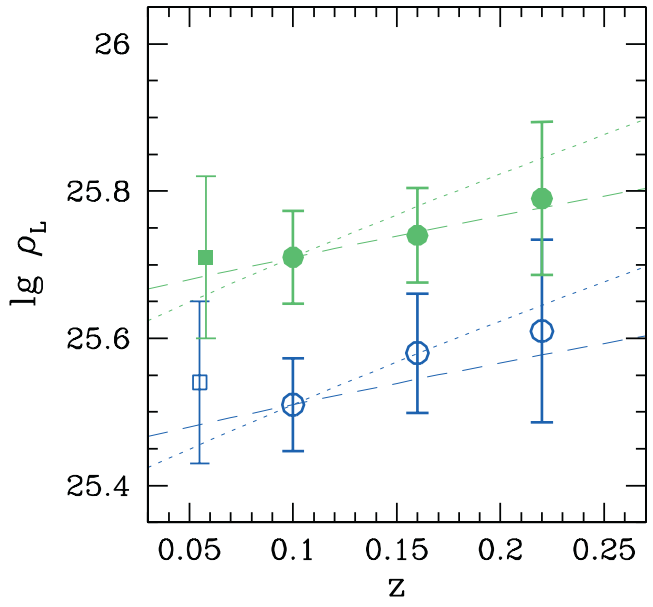

FIG. 4.—Luminosity density as a function of redshift in FUV (*blue open circles*) and NUV (*green filled circles*), along with local *GALEX* results (*squares*) by Wyder et al. (2005). The dotted and dashed lines correspond to $(1+z)^3$ and $(1+z)^{1.5}$, respectively, scaled to fit the lowest redshift bin of this study.

$(u'-r')_0$ discriminator, as all multicolor information is used. Figure 3 shows the FUV and NUV luminosity function for the early- and late-type galaxies. We find that M_* is brighter for the red population by approximately 0.2 mag in FUV and by 0.4 in NUV, and α is shallower than for the blue population by 0.3 (see Table 1). The marginalized errors on both M_* and α are large, but the difference between the joint distribution of parameters is significant (see insets of Fig. 3.) When using the rest-frame colors to split galaxies into red and blue, the plots exhibit the same features; the LFs at the faint end ($M \gtrsim -18$) are essentially indistinguishable, and the bright end is also consistent with the template-based results, although the difference is slightly less pronounced as expected, because of the larger scatter. The inverse concentration indices—simply the ratios of the radii containing 50% and 90% of the Petrosian r' fluxes—scatter significantly, but on average they are larger for galaxies in the blue class than the red ones; $C^{-1}_{\rm blue} = 0.46$ and $C^{-1}_{\rm red} = 0.42$. The red value is noticeably higher than that of the elliptical SDSS galaxies ($C^{-1} \approx 0.35$; Strateva et al. 2001), which indicates that our redder class too contains spiral galaxies.

3.2. *Luminosity Density*

We derive the mean luminosity density (LD) by integrating the luminosity with the Schechter function: $\rho_L = \int \phi(L) L\, dL = \phi_* L_* \Gamma(\alpha+2)$. In fact, the integral is calculated not just for the optimal fit, but over the whole range of parameters. Weighting the results by the probability [$w = \exp(-\chi^2/2)$] is essentially the same as using MC realizations for estimating the errors: $\delta\rho_L^2 = \langle\rho_L^2\rangle_w - \langle\rho_L\rangle_w^2$. Since the redshift range is limited, the error bars on the higher redshift bins are rather large. Table 1 shows the LD measurements, along with the statistical errors and estimates for the systematics due to cosmic variance that were derived similarly as in Wyder et al. (2005). As seen in Figure 4, both $\rho_{\rm FUV}$ and $\rho_{\rm NUV}$ increase with redshift and are consistent with $(1+z)^3$, and also $(1+z)^{1.5}$. The error bars in the figure are the combinations of the two sources of errors added in quadrature. They do not include errors from calibration uncertainties of ~10% that may account for $\delta \lg \rho_L = 0.04$ in both bands.

4. DISCUSSION

Using Two-Degree Field redshifts, the local *GALEX* studies by Wyder et al. (2005) and Treyer et al. (2005) derived very consistent results with the present findings. In the corresponding redshift ranges, the Schechter fits are mostly within the 68% confidence regions, with perhaps the one exception of M_* in NUV, which seems to be brighter, based on this photometric sample. The reason is that the different magnitude cuts in the UV yield slightly different galaxy populations, and our sample has more redder galaxies, which makes M_* brighter.

The LD measurements are also in good agreement with Wyder et al. (2005), and the observed trend is consistent with the *GALEX* Deep Imaging Survey results by Arnouts et al. (2005) and Schiminovich et al. (2005), probing the higher redshift universe out to $z = 1.2$. The evolution, in turn, is also consistent with results by Wilson et al. (2002), who find it to be proportional to $(1+z)^{1.7\pm1.0}$ for galaxies out to $z = 1.5$ at rest frame 2500 Å.

Going from the observed UV luminosity function to a SFR function is complicated by dust and the fact that the FUV and NUV light trace stars forming on different timescales. We will address this problem in subsequent *GALEX* papers.

GALEX (*Galaxy Evolution Explorer*) is a NASA small explorer launched in 2003 April. We gratefully acknowledge NASA's support for construction, operation, and science analysis for the *GALEX* mission, developed in cooperation with the Centre National d'Etudes Spatiales of France and the Korean Ministry of Science and Technology.

REFERENCES

Abazajian, K., et al. 2003, AJ, 126, 2081
Arnouts, S., et al. 2005, ApJ, 619, L43
Bruzual, G., & Charlot, S. 2003, MNRAS, 344, 1000
Choloniewski, J. 1986, MNRAS, 223, 1
Connolly, A. J., Csabai, I., Szalay, A. S., Koo, D. C., Kron, R. G., & Munn, J. A. 1995, AJ, 110, 2655
Connolly, A. J., Szalay, A. S., Dickinson, M., SubbaRao, M. U., & Brunner, R. J. 1997, ApJ, 486, L11
Cowie, L. L., Songaila, A., & Barger, A. J. 1999, AJ, 118, 603
Kennicutt, R. C., Jr. 1998, ARA&A, 36, 189
Lilly, S. J., Le Fèvre, Hammer, F., & Crampton, D. 1996, ApJ, 460, L1
Lynden-Bell, D., 1971, MNRAS, 155, 95
Martin, D. C., et al. 2005, ApJ, 619, L1
Milliard, B., Donas, J., Laget, M., Armand, C., & Vuillemin, A. 1992, A&A, 257, 24
Morrissey, P., et al. 2005, ApJ, 619, L7
Schechter, P. 1976, ApJ, 203, 297
Schiminovich, D., et al. 2005, ApJ, 619, L47
Schmidt, M. 1968, ApJ, 151, 393
Seibert, M., et al. 2005, ApJ, 619, L23
Strateva, I., et al. 2001, AJ, 122, 1861
Subbarao, M. U., Connolly, A. J., Szalay, A. S., & Koo, D. C. 1996, AJ, 112, 929
Treyer, M. A., et al. 2005, ApJ, 619, L19
Wilson, G., Cowie, L. L., Barger, A. J., & Burke, D. J. 2002, AJ, 124, 1258
Wyder, T. K., et al. 2005, ApJ, 619, L15
Xu, K., et al. 2005, ApJ, 619, L11